AIP | Applied Physics Letters

Parallel measurement of conductive and convective thermal transport of micro/nanowires based on Raman mapping

Man Li, Changzheng Li, Jianmei Wang, Xiangheng Xiao, and Yanan Yue

Citation: Applied Physics Letters **106**, 253108 (2015); doi: 10.1063/1.4923189
View online: http://dx.doi.org/10.1063/1.4923189
View Table of Contents: http://scitation.aip.org/content/aip/journal/apl/106/25?ver=pdfcov
Published by the AIP Publishing

Parallel measurement of conductive and convective thermal transport of micro/nanowires based on Raman mapping

Man Li,[1] Changzheng Li,[1] Jianmei Wang,[1] Xiangheng Xiao,[2] and Yanan Yue[1,a)]
[1]School of Power and Mechanical Engineering, Wuhan University, Wuhan, Hubei 430072, China
[2]Department of Physics, Wuhan University, Wuhan, Hubei 430072, China

(Received 7 April 2015; accepted 17 June 2015; published online 26 June 2015)

Heat conduction and convection are coupled effects in thermal transport of low-dimensional materials especially at micro/nanoscale. However, the parallel measurement is a challenge due to the limitation of characterization pathways. In this work, we report a method to study conductive and convective thermal transport of micro/nanowires simultaneously by using steady-state Joule-heating and Raman mapping. To examine this method, the carbon nanotubes (CNTs) fiber (36 μm in diameter) is characterized and its temperature dependence of thermal properties including thermal conductivity and convection coefficient in ambient air is studied. Preliminary results show that thermal conductivity of the CNTs fiber increases from 26 W/m K to 34 W/m K and convection coefficient decreases from 1143 W/m^2 K to 1039 W/m^2 K with temperature ranging from 312 to 444 K. The convective heat dissipation to the air could be as high as 60% of the total Joule heating power. Uncertainty analysis is performed to reveal that fitting errors can be further reduced by increasing sampling points along the fiber. This method features a fast/convenient way for parallel measurement of both heat conduction and convection of micro/nanowires which is beneficial to comprehensively understanding the coupled effect of micro/nanoscale heat conduction and convection. [http://dx.doi.org/10.1063/1.4923189]

Thermal transport in one-dimensional (1-D) structures has been studied extensively in the past two decades. The topics range from the fundamental understanding of thermophysical property[1] to the energy conversion applications, such as solar cell,[2] nanolaser,[3] and thermoelectric generator.[4,5] There are a few methods available for measuring heat conduction of wires, e.g., the 3ω method,[6,7] the transient electrothermal technique (TET),[8,9] and the microfabricated device method.[10] As an optical method, Raman spectroscopy has been widely used in the thermal characterization of low-dimensional materials, such as carbon nanotube (CNT), graphene, and other nanomaterials.[11–16] Yue *et al.* developed a steady-state method based on Raman spectroscopy for one-dimensional thermal characterization, namely, the steady-state electro-Raman-thermal (SERT) technique.[17] In this technique, the middle point temperature of the sample is monitored by Raman spectrum when the sample is heated by different steady-state currents. Thermal conductivity can be obtained from the linear relationship between Joule heating and the middle point temperature of the sample. The SERT technique has been applied to the thermal characterization of CNTs bundles and buckypapers.[17–19]

Among these methods as described above, a high vacuum environment is usually demanded to solely study heat conduction of the material. The extreme vacuum condition and difficulty in operating sample stages in a closed space drive us to develop a technique being capable of measuring samples in the air, that is, the heat convection effect is involved and needed to be considered accordingly. From the other point of view, the convection effect at micro/nanoscale is also important but was usually ignored in heat transfer analysis. Moreover, there is rare scenario for one-dimensional materials working in vacuum condition. For example, the CNTs-based materials used as thermoelectric devices,[20] thermal interface materials,[21] solar cells,[22] etc., are expected to work under ambient environment. Therefore, a comprehensive study of heat dissipation involving both heat conduction and convection is of great importance. In this paper, we report a method based on Raman thermometry to map temperature profile along the axial direction of the sample when it is heated by current. Different from SERT technique that only mid-point temperature is measured, this method records the temperature of several points which makes it possible to comprehensively analyze the convection heat dissipation to the air while studying the conduction along the sample. The heat conduction model considering convection effect is developed and the solution can be used in this parallel measurement of thermal conductivity and convection coefficient. Similar with SERT technique in Joule heating and Raman thermometry, this method also features steady-state, non-contact, and non-destructive measurement.

In the measurement, the wire suspended between two electrodes is heated by different constant currents. The sample ends remain at room temperature since electrodes have large heat capacity and high thermal conductivity. The heat mainly dissipates into the electrode through conduction and the air through convective heat transfer, which can be expressed mathematically as $d^2T/dx^2 + (Q - Q_{air})/kAL = 0$, where T represents temperature, x the distance from the middle point, Q the Joule-heating power, k the thermal conductivity, A the cross-sectional area, and L the length of the sample. The term Q_{air} stands for the convective heat transfer: $Q_{air} = hLS(T - T_0)$, where h is convection coefficient, S is wire perimeter, and T_0 is room temperature. Combined with

a)Email: yyue@whu.edu.cn

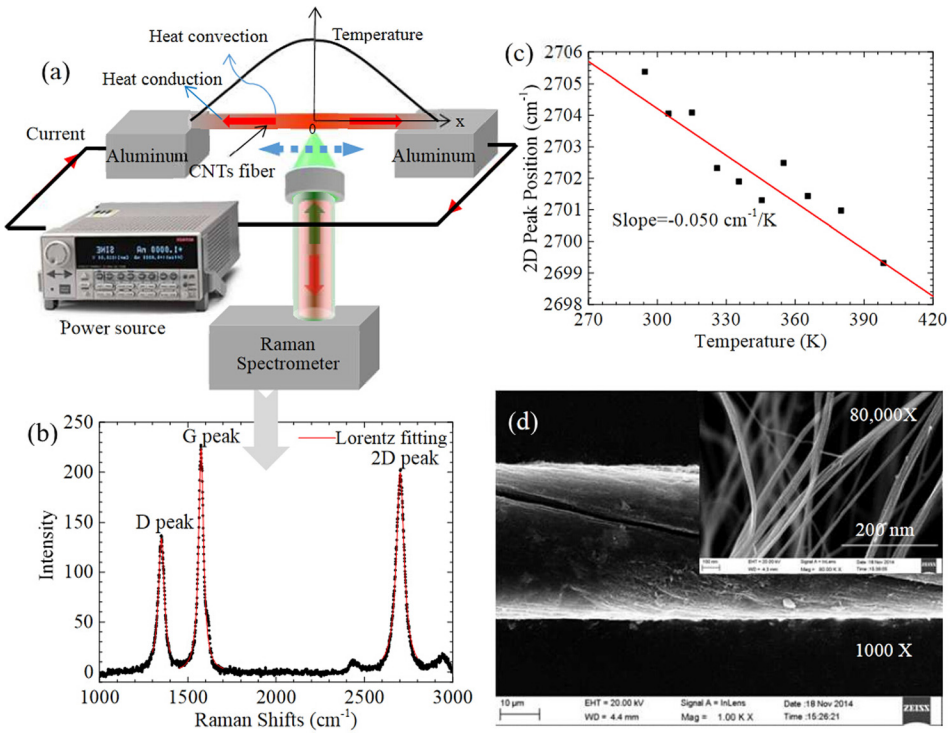

FIG. 1. (a) The schematic of steady-state Joule-heating-Raman-mapping technique for parallel characterization of thermal conductivity of CNTs fiber and heat convection coefficient. (b) The Raman spectrum of CNTs fiber at room temperature. (c) The linear fitting of the 2D peak positions with respect to temperature. (d) SEM images of the CNTs fiber, showing the side view of a perfect CNTs fiber; and the inset image displays the damaged surface at high magnification and the single carbon nanotube can be observed.

boundary conditions, the steady-state temperature distribution is solved as

$$T(x) = \frac{Q}{hLS}\left(1 - \frac{e^{\sqrt{hS/kA}x} + e^{-\sqrt{hS/kA}x}}{e^{\sqrt{hS/kA}L/2} + e^{-\sqrt{hS/kA}L/2}}\right) + T_0. \quad (1)$$

Figure 1(a) illustrates the schematic of experiment setup. In the experiment, the CNTs fiber is suspended between two aluminum electrodes. The ends of the sample are connected to the electrodes by highly conductive silver paste to minimize the electrical/thermal contact resistance. A current source (KEITHLEY 6220) is connected to the electrodes to supply constant currents to the fiber. Five points along the fiber ($x = 0$, $L/10$, $2L/10$, $3L/10$, $4L/10$) are chosen to measure its local temperature under different Joule-heating power from 25 mW to 97 mW. The local temperature is probed by noncontact Raman thermometry. Raman spectra along CNTs fiber are measured using LabRam HR confocal spectrometer (HORIBA Jobin Yvon Inc.), equipped with output laser energy less than 2.5 mW. Compared with the Joule heating power from 25 mW to 97 mW applied on the sample in the measurement, the amount of laser energy is negligible. Considering that there is reflection and scattering of the laser, the portion of laser energy absorption is even less. The exposure time is set as 15 s, the Raman shifts resolution is 0.89 cm^{-1}, and the objective lens used in the measurement is $\times 50$. A calibration experiment is conducted beforehand to get the linear relationship between Raman shift and temperature. The Raman spectrum is fitted with Lorentz function as shown in Fig. 1(b), and the slope of the 2D peak to the temperature is obtained as $-0.050\ cm^{-1}/K$ as shown in Fig. 1(c).

The CNTs fiber sample used in this work is from Nanjing JCNANO Company. The strength and modulus of the sample are 300–500 MPa and 50–100 GPa, respectively. As shown in Fig. 1(b), three peaks can be identified in the spectrum from 0 to 3000 cm^{-1}: the D-band $\sim 1350\ cm^{-1}$, the G-band $\sim 1580\ cm^{-1}$, and the 2D-band $\sim 2700\ cm^{-1}$. The scanning electron microscopy (SEM) images of the CNTs fiber as shown in Fig. 1(d) display the morphology and the hierarchic structure from the single inner tube to the whole fiber. The high ratio of the length (3.0 mm) to the diameter (36 μm) ensures one-dimensional thermal model applicable.

Figure 2 illustrates the temperature distribution along the fiber measured under different currents. By fitting the temperature profile using Eq. (1), the thermal conductivity of CNTs fiber is obtained with values from 26 W/m K to 34 W/m K for temperature ranging from 335 K to 468 K as shown in Fig. 3. This temperature-dependence effect cannot be explained by the phonon-phonon scattering (Umklapp) mechanism of crystalline materials. Since this CNTs fiber can be regarded as the

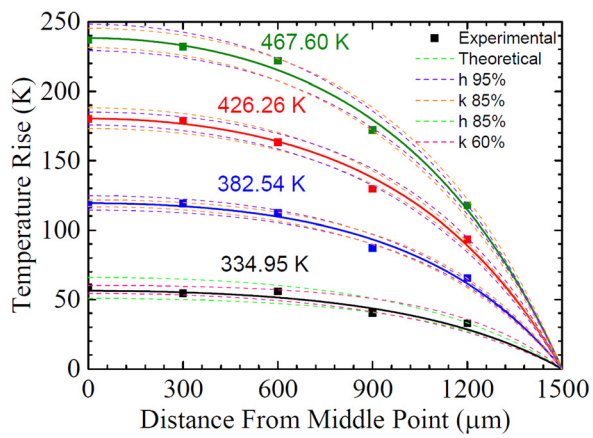

FIG. 2. The measured temperature rise at the points of $x = 0$ mm, 0.3 mm, 0.6 mm, 0.9 mm, 1.2 mm under different heating power and the fitting curves using Eq. (1). The marked temperature is the average temperature along the sample. The uncertainty of the value of k and h is analyzed by drawing theoretical curves with 95% h, 85% k, 85% h, and 60% k.

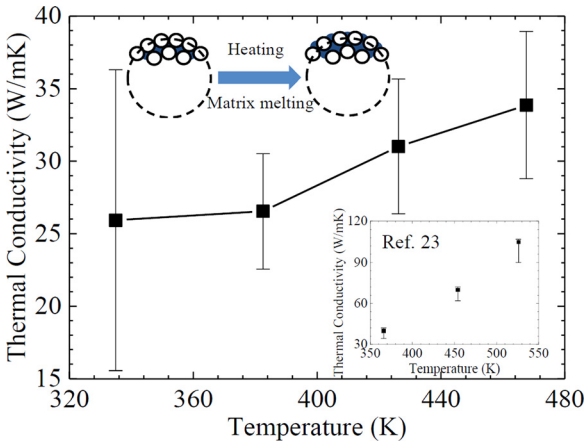

FIG. 3. The temperature dependence of thermal conductivity of the CNTs fiber, compared with the results in Ref. 23 as shown in the inset figure. The matrix becomes melted during the heating process. The volume of the CNTs fiber becomes larger because of the thermal expansion which might lead to the reduction in density. The sample surface turns to be smoother and thermal contact of CNT-CNT becomes better due to the melting of the organic matrix.

nanostructured composites (with organic matrix and lots of contacts), it is the inner structure and the matrix that determine its thermal property. When the temperature is increased, the solid phase of the matrix gradually turns to the liquid phase as illustrated in Fig. 3, which can improve the CNT-CNT thermal contact by additive adhesion force. The reduction in thermal contact resistance of CNT-CNTs leads to the increased thermal conductivity of CNTs fiber. The positive trend of thermal conductivity with respect to temperature was encountered in our previous measurement[23] as shown in the inset in Fig. 3. The previously reported thermal conductivity increased from 40 W/m K to 100 W/m K with temperature from 366 K to 526 K. The difference in thermal conductivity values between these two works stems from the difference in structure of the samples: the samples in previous work possess higher modulus of 600–800 MPa, suggesting better alignment and less defects.[23]

The TET thermal characterization is performed in vacuum condition for further structural analysis. The well-developed TET technique enables the accurate measurement of another important parameter: the thermal diffusivity $\alpha = k/\rho c_p$, which is equivalent to the ratio of thermal conductivity to the product of density and mass specific heat. More details and principle about the TET technique can be found in Refs. 8 and 23. The fitted thermal diffusivity is provided in Fig. 4(a), increasing from 1.51×10^{-5} to 3.12×10^{-5} m^2/s and from 312 K to 444 K. Taking the mass heat specific of graphite (709 J/kg K)[24] for a rough estimation, the mass density at different temperatures is plotted in Fig. 4(b). It shows that the mass density of the sample decreases from 2133 kg/m^3 to 1518 kg/m^3 with temperature from 335 K to 468 K. This value is lower than that of graphite (2100–2300 kg/m^3), and the decreased trend might stem from the melting of the glue matrix and the loose alignment of CNTS at high temperatures.

The convective heat transfer is of same importance as heat conduction for the heat dissipation of materials. However, for a long time, the study/characterization of h

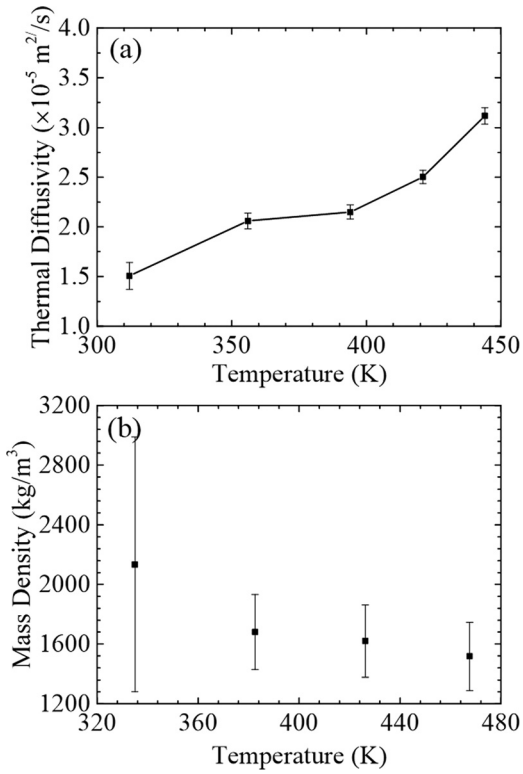

FIG. 4. (a) The fitted thermal diffusivity of our sample and its change with temperature from the TET experiment. (b) The density of the sample at different temperatures estimated from the measured thermal conductivity from Raman mapping experiment and thermal diffusivity from TET experiment.

(especially at micro/nanoscale) is challenging due to the complicated convective mechanism and the lack of measurement pathway for parallel characterization of heat conduction (k) and convection (h). Here, both k and h of micro/nanowires can be extracted from one fitting, which makes it possible for comprehensively understanding the coupled effect of convective and conductive heat transfer. As demonstrated in Fig. 5, the convection coefficient decreases from 1143 W/m^2 K to 1039 W/m^2 K monotonously for temperature from 335 K to 468 K. Heat convection coefficients measured here are larger than the normal values for large space (0–10 W/m^2 K for natural convection). It is because the heat convection behaves more like conduction effect at micro/

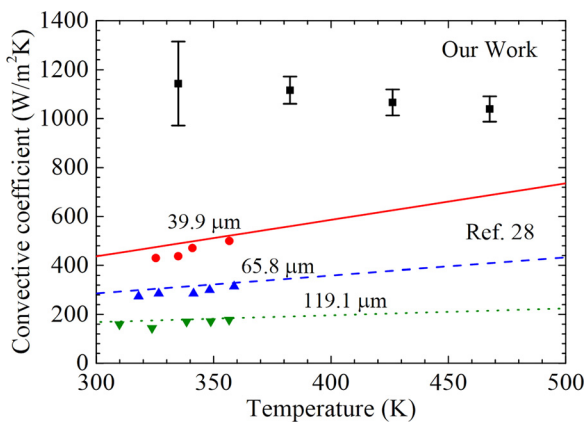

FIG. 5. The temperature dependence of convection coefficient for the fiber in the air, in comparison with the referenced experimental and simulated data previously reported for copper microwire.[28]

TABLE I. Effects of intrinsic temperature and diameter of fiber on its convection coefficient.

Temperature (K)	Density (kg/m^3)	Diameter (μm)	h change caused by T (W/m^{2}K)	h change caused by D (W/m^{2}K)	Total change (W/m^{2}K)
335	2134	36.6	63	−2	61
383	1680	41.2	134	−18	116
426	1620	42.0	199	−21	178
468	1518	43.3	261	−26	235

nanoscale due to the limitation of energy exchange between sample and air molecules. The empirical equation for microscale space $h = (2.68 + 0.11/\sqrt{D})^2$ for $10\,\mu\text{m} < D < 10\text{m}$,[25] which has been widely adopted to analyze the thermal management problems involving microscale heat convection,[26,27] gives a value of 274 W/m^{2}K. Considering that the surface microstructure of the sample can greatly improve the total surface area, our result of ~1100 W/m^{2}K is comparable with the predicted value. Similar results have been obtained in previous studies: the convection coefficient was measured as 400–500 W/m^{2}K for copper microwire (39.9 μm)[28] and ~400 W/m^{2}K for platinum microwire (32.6 μm).[29] The ultrahigh value of h indicates the non-negligible energy dissipation through heat convection, which can actually be estimated according to the mapped temperature profile and the fitted h. For example, when the heating power is 97 mW, the heat convection can be calculated as $Q_{air} = \int \pi D h(T - T_0)dx = 59.4\,\text{mW}$, which is about 60% of the total energy.

The temperature dependence of h comes from two factors: one is the direct temperature effect, reflecting the physical property change of the air and fiber, e.g., thermal diffusivity and viscosity of air; and the other one is the indirect temperature factor, i.e., thermal expansion effect and matrix melting during the heating, which change the inner microstructure. The direct temperature and diameter dependence of convection coefficient for metal microwires have been studied by Guan *et al.*[28] Using their experimental and theoretical data, the relationship between diameter and h can be approximately linearly fitted as $h = -3.55 \times 10^{-6}D + 575.32$, where D is diameter, and the relationship between temperature and h can be fitted as $h = 1.496T - 12.237$, T is the absolute temperature. The direct effects of temperature and diameter change on the heat convection coefficient are listed in Table I. The diameters are calculated based on $D/D_0 = (\rho_0/\rho)^{1/2}$, where the initial diameter is 36 μm and the initial density of the fiber is assumed as 2200 kg/m^3 (graphite). The power factor 1/2 is from the assumption that the length remains unchanged. It can be found in Table I that although the diameter gives the negative temperature dependence, the temperature can give positive effect. Slightly negative temperature dependence of convection coefficient in our work is different with the result of Guan *et al.*, which is caused by the composites of our CNTs fiber. Compared with copper wire, the structure of CNTs fiber is much more complex. As shown in Fig. 3, the solid matrix becomes melted at high temperatures and the liquid matrix can wet the individual carbon nanotubes. Some of the grooves on the surface will be filled with the liquid matrix, leading to a smoother surface. The convection coefficient (effective) decreases when the specific surface area is reduced. Therefore, it might not be the direct effect of the temperature but the inner structural change of CNTs fiber that leads to the negative temperature dependence of the convection coefficient. Further effort will be devoted to exploring the mechanism of this phenomenon.

The uncertainty of experimental results (k and h) is introduced mainly in the fitting process by using Eq. (1). Based on Taylor's expansion of $e^x + e^{-x} = 2 + 2\sum_{i=1}^{\infty} x^{2i}/(2i)!$ and the term $\sqrt{hS/kA}x \le \sqrt{hS/kA}L/2 < 3$, the terms higher than second order can be approximately neglected. The fitting equation can be simplified as

$$T(x) = \frac{Q}{hLS}\left(1 - \frac{1 + hSx^2/2kA}{1 + hSL^2/8kA}\right) + T_0. \tag{2}$$

The convection coefficient (h) and thermal conductivity (k) can be written as

$$h = \frac{Q}{\pi LD(T - T_0)} - \frac{4Qx^2}{\pi L^3 D(T - T_0)} - \frac{2kD}{L^2}, \tag{3}$$

$$k = \frac{QL}{2\pi D^2(T - T_0)} - \frac{2Qx^2}{\pi LD^2(T - T_0)} - \frac{hL^2}{2D}. \tag{4}$$

As seen from these equations, the uncertainty is mainly from the heating power (Q), diameter (d) and length of the fiber (L), temperature rise (T), and position of the measurement points (x). In the experiment, the applied current is stable. As to the fiber length and the measurement positions, the spatial resolution is as high as 10 μm and the multi-points fitting would further eliminate the uncertainty. Thus, the diameter and the resolution of Raman thermometry introduce the most measurement uncertainties. The resolution of Raman shift is 0.89 cm^{-1}, and the Lorentz fitting can reduce the uncertainty to 0.3 cm^{-1} within the confidence interval of 95%, which means the uncertainty of Raman thermometry is 6 K. From the SEM images of our sample, we observed the diameter ranging from 33 μm to 38 μm. In the measurement, the uncertainty of diameter should be much less than 3 μm since the value involved in the calculation is an averaged value through the whole sample length, say, 1 μm. The uncertainty of h and k can be evaluated according to the following equations: $\Delta h = |(\partial h/\partial T)\cdot\Delta T| + |(\partial h/\partial D)\cdot\Delta D|$, $\Delta k = |(\partial k/\partial T)\cdot\Delta T| + |(\partial k/\partial D)\cdot\Delta D|$. The data with the average temperature of 426 K are chosen for the uncertainty analysis as an example. Applying conditions: heating power 75 mW, sample length 3 mm, average diameter 36 μm, the distance of the local temperature 0.3 mm, local temperature rise 179 K, the fitted h and k: 1066 W/m^{2}K and 31 W/mK, and the uncertainties are calculated as 69 W/m^{2}K for h and 8.5 W/mK for k. Besides, these uncertainties are from the calculation by using the data of one point. In this measurement, the thermal

property parameters are fitted by using the local temperature of five points, thus the uncertainty can be reduced to 31 W/m^2K and 3.8 W/m K. It can be further reduced by taking account of more points.

In summary, the parallel measurement of conductive and convective thermal transport is accomplished in this work upon CNTs fiber. A method is established to simultaneously characterize thermal conductivity and convection coefficient of micro/nanowires by using Raman mapping along the axial of the sample. By fitting experimental data with the physical model developed in this work, the thermal conductivity and convection coefficient are measured, respectively, as 26 W/m K to 34 W/m K and 1143 W/m^2K to 1039 W/m^2K with temperature from 335 K to 468 K. The defects and the CNTs interface are responsible for the low thermal conductivity. And the super high specific surface area caused by the tremendous grooves on the surface leads to the high convection coefficient. Besides, the positive temperature dependence of thermal conductivity and the negative temperature dependence of convection coefficient is observed. Preliminary analysis is conducted and this phenomenon is attributed to the possible structural change in the CNTs fiber during the heating experiment.

Y.Y. would like to thank the financial support by National Natural Science Foundation of China (Nos. 51206124 and 51428603). X.X would like to thank the National Natural Science Foundation of China (Nos. U1260102 and 51371131).

[1]S. Lepri, R. Livi, and A. Politi, Phys. Rep. **377**, 1 (2003).
[2]E. C. Garnett, M. L. Brongersma, Y. Cui, and M. D. McGehee, Annu. Rev. Mater. Res. **41**, 269 (2011).
[3]M. H. Huang, S. Mao, H. Feick, H. Yan, Y. Wu, H. Kind, E. Weber, R. Russo, and P. Yang, Science **292**, 1897 (2001).
[4]A. I. Hochbaum, R. Chen, R. D. Delgado, W. Liang, E. C. Garnett, M. Najarian, A. Majumdar, and P. Yang, Nature **451**, 163 (2008).
[5]A. I. Boukai, Y. Bunimovich, J. Tahir-Kheli, J.-K. Yu, W. A. Goddard III, and J. R. Heath, Nature **451**, 168 (2008).
[6]D. G. Cahill, Rev. Sci. Instrum. **61**, 802 (1990).
[7]D. G. Cahill and R. O. Pohl, Phys. Rev. B **35**, 4067 (1987).
[8]J. Guo, X. Wang, and T. Wang, J. Appl. Phys. **101**, 063537 (2007).
[9]M. Li, Y. Sun, H. Xiao, X. Hu, and Y. Yue, Nanotechnology **26**, 105703 (2015).
[10]L. Shi, D. Li, C. Yu, W. Jang, D. Kim, Z. Yao, P. Kim, and A. Majumdar, J. Heat Transfer **125**, 881 (2003).
[11]Z. Yan, C. Jiang, T. R. Pope, C. F. Tsang, J. L. Stickney, P. Goli, J. Renteria, T. T. Salguero, and A. A. Balandin, J. Appl. Phys. **114**, 204301 (2013).
[12]H. Malekpour, K. H. Chang, J. C. Chen, C. Y. Lu, D. L. Nika, K. S. Novoselov, and A. A. Balandin, Nano Lett. **14**, 5155 (2014).
[13]Z. Yan, D. L. Nika, and A. A. Balandin, in *IET Circuits, Devices and Systems* (Institution of Engineering and Technology, 2015), Vol. 9, p. 4.
[14]A. A. Balandin, Nat. Mater. **10**, 569 (2011).
[15]A. A. Balandin, S. Ghosh, W. Bao, I. Calizo, D. Teweldebrhan, F. Miao, and C. N. Lau, Nano Lett. **8**, 902 (2008).
[16]S. Ghosh, W. Bao, D. L. Nika, S. Subrina, E. P. Pokatilov, C. N. Lau, and A. A. Balandin, Nat. Mater. **9**, 555 (2010).
[17]Y. Yue, G. Eres, X. Wang, and L. Guo, Appl. Phys. A **97**, 19 (2009).
[18]Y. Yue, X. Huang, and X. Wang, Phys. Lett. A **374**, 4144 (2010).
[19]M. Li and Y. Yue, J. Nanosci. Nanotechnol. **15**, 3004 (2015).
[20]J. Chen, X. Gui, Z. Wang, Z. Li, R. Xiang, K. Wang, D. Wu, X. Xia, Y. Zhou, Q. Wang, Z. Tang, and L. Chen, ACS Appl. Mater. Interfaces **4**, 81 (2011).
[21]J. Xu and T. S. Fisher, Int. J. Heat Mass Transfer **49**, 1658 (2006).
[22]T. Chen, L. Qiu, Z. Cai, F. Gong, Z. Yang, Z. Wang, and H. Peng, Nano Lett. **12**, 2568 (2012).
[23]Y. Yue, K. Liu, M. Li, and X. Hu, Carbon **77**, 973 (2014).
[24]E. Pop, V. Varshney, and A. K. Roy, MRS Bull. **37**, 1273 (2013).
[25]J. Peirs, D. Reynaerts, and H. Van Brussel, "Scale effects and thermal considerations for micro-actuators," in *Proceedings of the IEEE International Conference on Robotics and Automation* (IEEE, 1998), p. 1516.
[26]A. K. Sokół and R. P. Sarzała, Opto-Electron. Rev. **21**, 191 (2013).
[27]A. Giberti, V. Guidi, and D. Vincenzi, Sens. Actuators, B **153**, 409 (2011).
[28]N. Guan, Z. Liu, C. Zhang, and G. Jiang, Heat Mass Transfer **50**, 275 (2014).
[29]Z. L. Wang and D. W. Tang, Int. J. Therm. Sci. **64**, 145 (2013).